

# Benzoate Cyclometalation Enables Oxidative Addition of Haloarenes at a Ru(II) Center

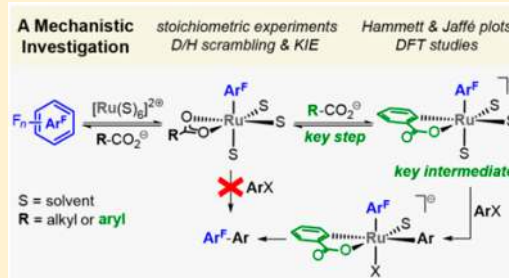
Marco Simonetti,<sup>†</sup> Rositha Kuniyil,<sup>‡</sup> Stuart A. Macgregor,<sup>\*,†,‡,Ⓛ</sup> and Igor Larrosa<sup>\*,†,‡,Ⓛ</sup>

<sup>†</sup>School of Chemistry, University of Manchester, Oxford Road, Manchester M13 9PL, U.K.

<sup>‡</sup>Institute of Chemical Sciences, Heriot-Watt University, Edinburgh EH14 4AS, U.K.

**S** Supporting Information

**ABSTRACT:** The first Ru(II)-catalyzed arylation of substrates without a directing group was recently developed. Remarkably, this process only worked in the presence of a benzoate additive, found to be crucial for the oxidative addition step at Ru(II). However, the exact mode of action of the benzoate was unknown. Herein, we disclose a mechanistic study that elucidates the key role of the benzoate salt in the C–H arylation of fluoroarenes with aryl halides. Through a combination of rationally designed stoichiometric experiments and DFT studies, we demonstrate that the aryl–Ru(II) species arising from initial C–H activation of the fluoroarene undergoes cyclometalation with the benzoate to generate an anionic Ru(II) intermediate. The enhanced lability of this intermediate, coupled with the electron-rich anionic Ru(II) metal center renders the oxidative addition of the aryl halide accessible. The role of an additional (NMe<sub>4</sub>)OC(CF<sub>3</sub>)<sub>3</sub> additive in facilitating the overall arylation process is also shown to be linked to a shift in the C–H pre-equilibrium associated with benzoate cyclometalation.

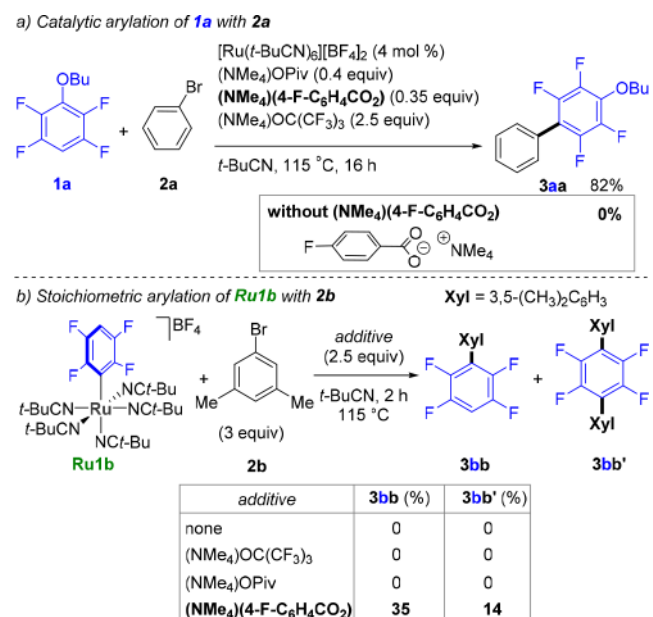


## 1. INTRODUCTION

The polyfluorobiphenyl unit is a recurrent building block found as a structural component in drugs,<sup>1a–c</sup> agrochemicals,<sup>1e,f</sup> and numerous functional materials<sup>1g–m</sup> such as organic light-emitting diodes (OLEDs)<sup>1j</sup> and liquid crystals.<sup>1k,i</sup> Although cross-coupling methods can be applied to access these biaryl moieties,<sup>2</sup> C–H arylation strategies have been acknowledged as a more sustainable alternative strategy to selectively form aryl–aryl bonds.<sup>3</sup> In this context, fluorinated biaryls can be generated under Pd catalysis employing fluoroarenes with coupling partners such as aryl (pseudo)-halides,<sup>4a–d</sup> aryl boronic donors,<sup>4e</sup> or simple arenes.<sup>4f,g</sup> Alternatively, Cu-<sup>5</sup> or Au-catalysts<sup>6</sup> can be used to promote analogous transformations. Recently, our group expanded upon the range of transition metal catalysts able to promote this particular type of coupling.<sup>7</sup> The arylation of fluoroarenes with aryl halides occurred with a Ru(II) catalyst, [Ru(*t*-BuCN)<sub>6</sub>][BF<sub>4</sub>]<sub>2</sub>, aided by (NMe<sub>4</sub>)OPiv and (NMe<sub>4</sub>)(4-F-C<sub>6</sub>H<sub>4</sub>CO<sub>2</sub>) cocatalysts and (NMe<sub>4</sub>)OC(CF<sub>3</sub>)<sub>3</sub> base in *t*-BuCN (Scheme 1a). Notably, this methodology is the first Ru-catalyzed C–H arylation process operating without the need for a directing group in the arene.

Crucially, this Ru-catalyzed C–H arylation only proceeded when a benzoate salt was present, with all other bases and carboxylates tested unable to switch on the reaction. Indeed, when the arylation of polyfluoroarene **1a** was carried out in the absence of the benzoate additive, no cross-coupled product **3aa** was formed. To further clarify the surprising role of the benzoate source, a stoichiometric arylation between the

## Scheme 1. Importance of the Benzoate Additive in the Ru-Catalyzed Arylation of Fluorobenzenes



catalytically active intermediate tetrafluorophenyl–Ru(II) complex **Ru1b** and 5-bromo-*m*-xylene **2b** was performed

Received: July 31, 2018

Published: August 22, 2018

(Scheme 1b). Biaryls **3bb** and **3bb'** were formed *only when the benzoate was added*. Remarkably, the structurally related pivalate salt did not promote the transformation. These empirical results, along with mechanistic studies and DFT calculations, led us to suggest a catalytic cycle where, although the initial C–H activation of the fluoroarene is assisted by pivalate, the formal oxidative addition of the aryl halide could only proceed when benzoate was present.<sup>7</sup> However, the mechanism by which benzoate may facilitate oxidative addition remained unknown.

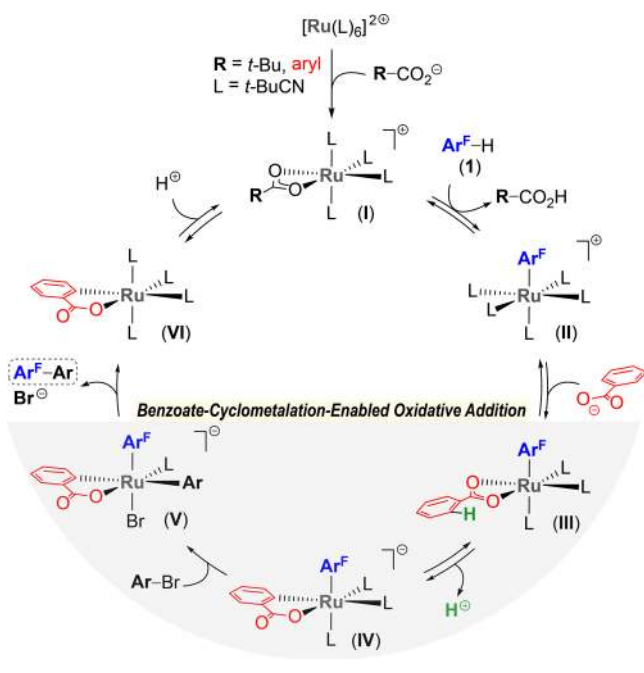
Herein, we report mechanistic studies elucidating the role of the benzoate salt. Our experiments demonstrate that aryl–Ru(II) species such as **Ru1b**, which are inert toward oxidative addition with aryl bromides **2**, can undergo cyclometalation with the benzoate salt to form an anionic Ru(II) intermediate that is highly reactive toward oxidative addition and is essential to the reactivity of the system. In a similar vein, we have also recently proposed that the mechanism of the Ru(II)-catalyzed C–H arylation of N-chelating substrates with aryl (pseudo)-halides involves a bis-cyclometalated Ru(II) species as the key intermediate required for oxidative addition to occur.<sup>8</sup>

## 2. RESULTS AND DISCUSSION

### 2.1. Mechanistic Hypothesis for the Role of the Benzoate.

The specific requirement for a benzoate salt for the reaction to proceed led us to hypothesize that the benzoate may be undergoing *ortho*-C–H activation as its mode of action. Scheme 2 outlines our proposed catalytic cycle for the

Scheme 2. Proposed Catalytic Cycle



process. After the initial C–H activation of the fluoroarene **1** to form the cationic fluoroaryl–Ru(II) complex **II**, a second C–H activation event on the benzoate would generate anionic Ru(II)-species **IV** featuring a cyclometalated benzoate unit. This more electron-rich Ru(II) intermediate **IV** would be more reactive toward oxidative addition with the aryl halide (to **V**) than the cationic complex **II** or the neutral species **III**. Reductive elimination from **V** would then produce the biaryl product. In contrast, an aliphatic carboxylate such as pivalate

would be unable to undergo cyclometalation and thus would be unable to promote the desired arylation reaction. Indeed, whereas the cyclometalation of aromatic benzoates by Ru(II) complexes is well-known and recognized,<sup>9,10</sup> the more challenging  $\beta$ -cyclometalation of aliphatic carboxylic acids has yet to be observed.

### 2.2. Kinetic and Isotopic Studies.

With this mechanistic framework in mind and given the possibility of isolating cationic intermediate **II**, we decided to examine stoichiometric arylation reactions to directly probe the cyclometalation and the oxidative addition steps without interference from the initial C–H activation of the fluoroarene (from **I** to **II**, Scheme 2). Thus, we started investigating the kinetic profile of the coupling of pentafluorophenyl–Ru(II) species **Ru1c** with bromoarene **2b** in the presence of a variety of benzoate derivatives (Figure 1). In order to standardize the measure-

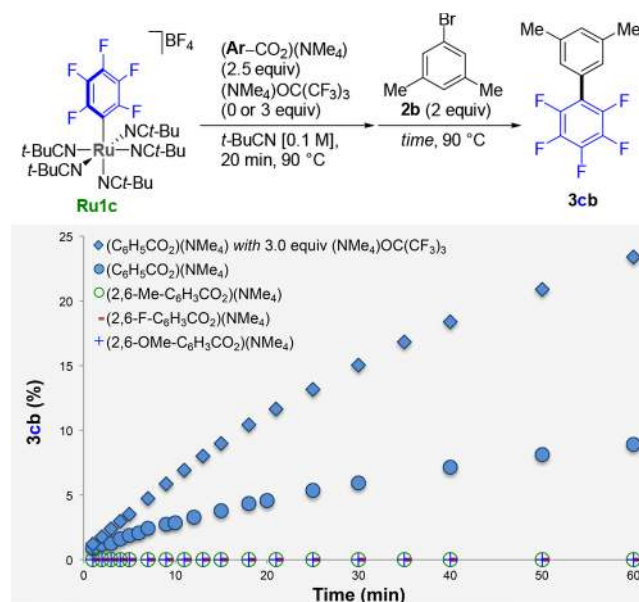
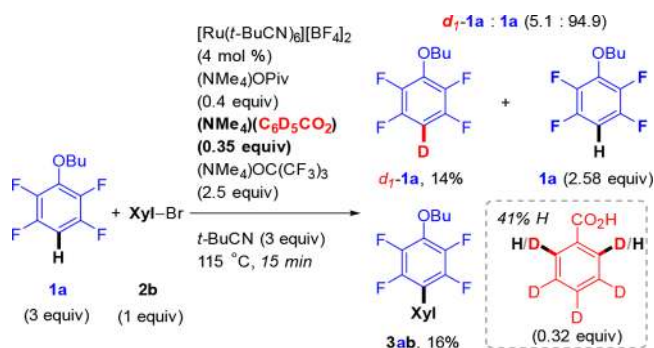


Figure 1. Stoichiometric arylation of **Ru1c** with **2b** employing  $(\text{NMe}_4)$ -2,6-disubstituted benzoates or simple benzoate in the presence or in the absence of  $(\text{NMe}_4)\text{OC}(\text{CF}_3)_3$  base. Yield determined by GC-FID using hexadecane as internal standard.

ments, **Ru1c** was preincubated for 20 min at 90 °C with the benzoate salt prior to the addition of **2b**. In agreement with our hypothesis, 2,6-disubstituted benzoate sources, which cannot undergo *ortho*-C–H activation, did not give any biaryl **3cb** irrespective of the electronic effect of these groups (Me, F, OMe). Instead, paralleling our previous observations,  $(\text{NMe}_4)$ - $(\text{C}_6\text{H}_5\text{CO}_2)$  triggered the desired coupling. In view of the often reversible nature of the C–H activation in Ru(II) catalysis,<sup>11</sup> we predicted that the addition of an external base would shift the equilibrium **III**–**IV** toward **IV** (Scheme 2), thus enhancing the reactivity. Indeed, when  $(\text{NMe}_4)$ - $(\text{C}_6\text{H}_5\text{CO}_2)$  was used in combination with the base  $(\text{NMe}_4)\text{OC}(\text{CF}_3)_3$ , a conspicuous acceleration of the rate of arylation was obtained.<sup>12</sup> These data strongly suggest that the proposed *ortho*-metalation to generate intermediate **IV** is a key step en route to the formation of the aryl–aryl bond.

In order to test this hypothesis further, catalytic arylation of nonvolatile polyfluoroarene **1a** with bromoarene **2b** was carried out utilizing the deuterated  $(\text{NMe}_4)(\text{C}_6\text{D}_5\text{CO}_2)$  under standard optimized reaction conditions<sup>7</sup> (Scheme 3).

**Scheme 3. Catalytic Arylation of 1a with Bromoarene 2b Employing (NMe<sub>4</sub>)C<sub>6</sub>D<sub>5</sub>CO<sub>2</sub><sup>a</sup>**


<sup>a</sup>Xyl = 3,5-dimethylphenyl.

Analysis of the reaction mixture after 15 min revealed the formation of biaryl **3ab** in 16% yield. More importantly, recovered fluoroarene **1a** showed 14% deuteration, and recovered benzoic acid revealed a 41% H enrichment at the *ortho* positions. Since the only source of D was the benzoate salt, this experiment highlights the reversible nature of the steps from intermediate I to IV of the catalytic cycle (Scheme 2) and provides further evidence for the cyclometalation of the benzoic acid. Unfortunately, all attempts at isolation or *in situ* detection of IV starting from Ru1c in the presence of benzoate salts were unsuccessful, and this likely reflects the high energy of intermediate IV (see SI, section 5 for details and DFT studies below).

Subsequently, we set out to investigate whether a KIE was associated with the benzoate cyclometalation step. The initial arylation rates of two independent stoichiometric couplings of pentafluorophenyl-containing Ru1c (intermediate II in Scheme 2) with 5-bromo-*m*-xylene **2b** using either (NMe<sub>4</sub>)-(C<sub>6</sub>H<sub>5</sub>CO<sub>2</sub>) or (NMe<sub>4</sub>)-(C<sub>6</sub>D<sub>5</sub>CO<sub>2</sub>) were therefore recorded (Figure 2). The rate of formation of biaryl **3cb** with the

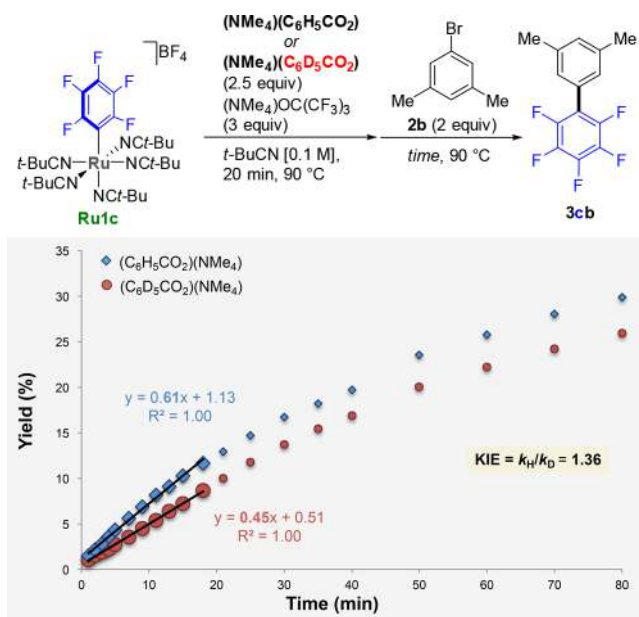
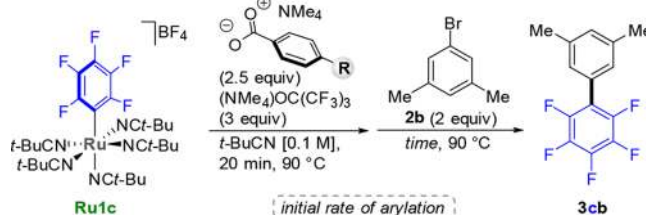


**Figure 2.** Stoichiometric arylation of Ru1c with **2b** employing (NMe<sub>4</sub>)-(C<sub>6</sub>H<sub>5</sub>CO<sub>2</sub>) or (NMe<sub>4</sub>)-(C<sub>6</sub>D<sub>5</sub>CO<sub>2</sub>) and (NMe<sub>4</sub>)OC(CF<sub>3</sub>)<sub>3</sub>. Yield determined by GC-FID using hexadecane as internal standard.

benzoate source was 1.36 times faster than the one with the perdeuterated benzoic salt, suggesting that the cyclometalation of the benzoate (III to IV in Scheme 2) is kinetically relevant and likely an equilibrium under the reaction conditions.<sup>13</sup>

**2.3. Hammett and Jaffé Plots.** In order to gain further mechanistic insights into the cyclometalation step of the benzoate additive, we compared the initial rates of formation of biaryl **3cb** in the stoichiometric arylation reactions of Ru1c with **2b** in the presence of a variety of electronically diverse 4-substituted benzoate salts (Table 1).<sup>14</sup> First, and surprisingly,

**Table 1. Hammett Plots: Initial Rates Data of the Arylation of Ru1c with Bromoarene 2b Employing Different 4-Substituted Benzoates<sup>a</sup>**



Entry	$\sigma_m$	$\sigma_p$	$k_{obs}$ (%/min)	$\log(k/k_a)$	
1	NMe <sub>2</sub>	-0.16	-0.83	1.7334	0.4906
2	<i>t</i> -Bu	-0.10	-0.20	0.7858	0.1470
3	Me	-0.07	-0.17	0.7283	0.1140
4	H	0	0	0.5602	0
5	CH <sub>2</sub> CN	0.16	0.18	1.0770	0.2839
6	C <sub>6</sub> F <sub>5</sub>	0.26	0.27	1.8236	0.5126
7	OCF <sub>3</sub>	0.38	0.35	2.5290	0.6546
8	CF <sub>3</sub>	0.43	0.54	2.7943	0.6979
9	OMe	0.12	-0.27	1.7610	0.4974
10	OEt	0.10	-0.24	1.5220	0.4341
11	OPh	0.25	-0.03	2.4571	0.6411
12	F	0.34	0.06	1.7222	0.4877

<sup>a</sup>Stoichiometric arylation of Ru1c with **2b** employing *para*-substituted (NMe<sub>4</sub>)-benzoates and (NMe<sub>4</sub>)OC(CF<sub>3</sub>)<sub>3</sub> base. Initial arylation rates in formation of **3cb** were determined by GC-FID using hexadecane as internal standard.

the rate of arylation ( $k_{obs}$ ) increased with both electron-rich and electron-poor benzoates, with the parent unsubstituted benzoate displaying the slowest rate. A second observation from these data can be extracted from the corresponding Hammett plots (Figure 3).<sup>15</sup> Since both *meta* and *para* positions to the substituent are potentially involved in the process, we plotted  $\log(k_X/k_H)$  versus both  $\sigma_m$  and  $\sigma_p$ . In both plots most substituents fit well to a V-shaped Hammett plot (blue diamonds), suggesting that there are both *meta* and *para* effects. Interestingly, there are four clear outliers (red circles and green triangles). From the  $\sigma$  constants of the groups studied, it can be seen that those highlighted in blue have similar  $\sigma_m$  and  $\sigma_p$  values. In contrast, the groups in red and green have significantly different values for their  $\sigma_m$  and  $\sigma_p$  constants. For example, the OMe and OEt groups have negative  $\sigma_p$  values (-0.27, -0.24) but positive  $\sigma_m$  (0.12, 0.10). These two groups show higher reactivity than would be expected from Figure 3, where only their  $\sigma_m$  or  $\sigma_p$  are



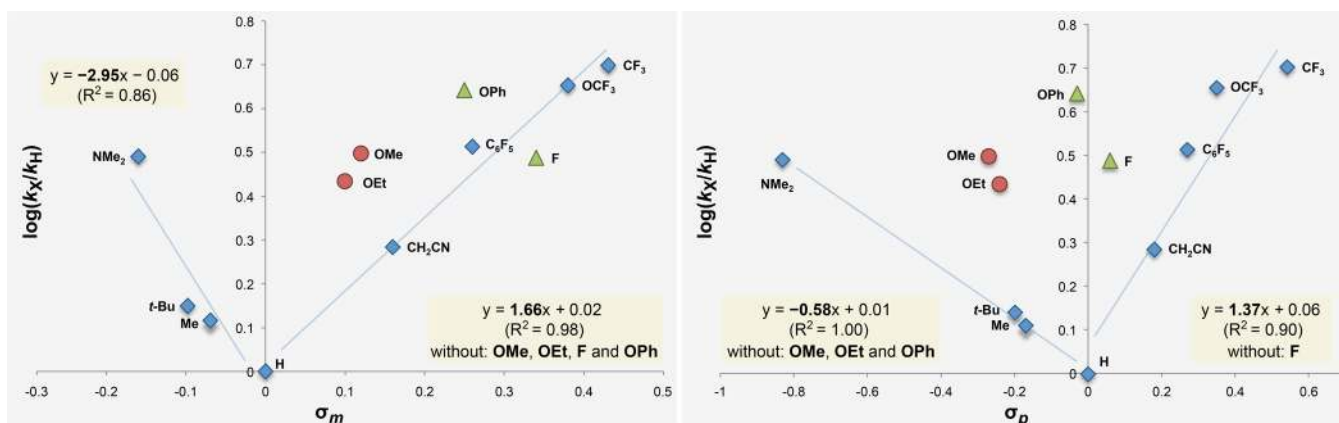


Figure 3. Evaluation of benzoate electronic effect on rate. Hammett plots:  $\log(k_X/k_H)$  vs  $\sigma_m$  (left) and  $\sigma_p$  (right).

considered in isolation. This implies that opposite electronic effects are synergistically combining to lower the overall  $\Delta G^\ddagger$ , thus enhancing the arylation rate. These observations indicate that both  $\sigma_m$  and  $\sigma_p$  must be considered at the same time. This is reasonable in the system under study as both the kinetically relevant cyclometalation (III to IV) and the rate-limiting aryl bromide oxidative addition (IV to V) steps may be affected by electronic perturbation at the *meta* and *para* sites of the benzoate substrates ( $C_{Ar}-H$  ( $\sigma_m$ ),  $C(O)O^-/H$  ( $\sigma_p$ ),  $C_{Ar}-[Ru]$  ( $\sigma_m$ ),  $C(O)O-[Ru]$  ( $\sigma_p$ )) at several points in the arylation process (Figure 4). We return to deconvolute these

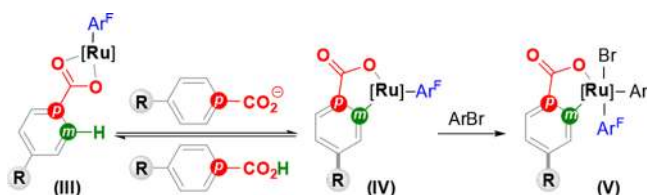


Figure 4. Influence of the R group on the electronic properties at multiple *meta* and *para* positions affecting the kinetically relevant cyclometalation, as well as the oxidative addition step.

*meta* and *para* effects in the computational section below. Importantly, considering the Hammett equation, eq 1, a Hammett plot should only result in a linear free energy relationship (LFER) if the electronic influence of the R group affects only one position of the aromatic (*meta* or *para*) of a kinetically relevant step (i.e., if  $\rho_p\sigma_p \gg \rho_m\sigma_m$  or  $\rho_m\sigma_m \gg \rho_p\sigma_p$ ).

Hammett equation:

$$\log\left(\frac{k_X}{k_H}\right) = \rho_m\sigma_m + \rho_p\sigma_p \quad (1)$$

Although V-shaped Hammett plots are usually associated with a change in the mechanism of the process,<sup>16</sup> the lowering of the overall  $\Delta G^\ddagger$  due to a weighed variation of the electronic properties of the *meta* and *para* positions of the benzoates associated with the kinetically relevant cyclometalation provides a more logical explanation for our experimental data (see also the DFT studies below). To validate further this hypothesis, we applied Jaffé's analysis of the Hammett equation to our system. This modification allows the correlation of substituent perturbations that influence more than one reactive center at the same time to be plotted (Figure 5).<sup>17</sup> In the Jaffé equation, the Hammett equation is divided by one of the two  $\sigma$  values. Depending on which  $\sigma$  constant is in the denominator, the slope of the plot gives one  $\rho$  value, while the  $y$ -intercept provides the other  $\rho$  value (eqs 2 and 3). In order to verify the LFER, both plots should result in the same values of  $\rho_m$  and  $\rho_p$ . As shown in Figure 5, this treatment of the data led to two plots showing a LFER valid for all the substituents. Similar  $\rho$  values were obtained in both cases ( $\rho_m \cong 2.2$ ;  $\rho_p \cong -1.2$ ), thus validating our mechanistic framework. The magnitude of the  $\rho$  values indicates that the electronic perturbation on the  $C_{Ar}-H/[Ru]-C_{Ar}$  bonds (i.e., *meta*) has a greater effect on the overall rate. Furthermore, the signs of  $\rho_m$  and  $\rho_p$  indicate that the overall rate is enhanced by *para*-EDGs

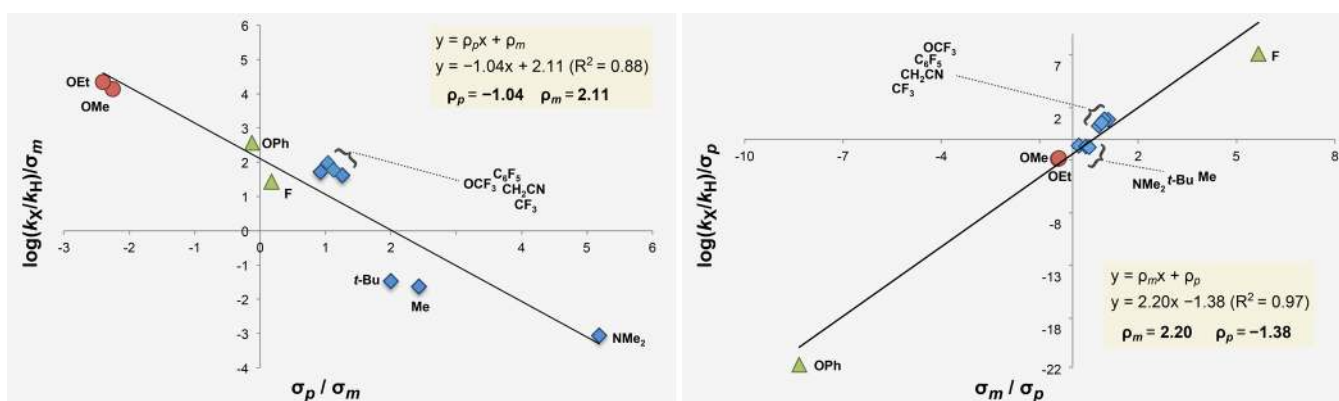
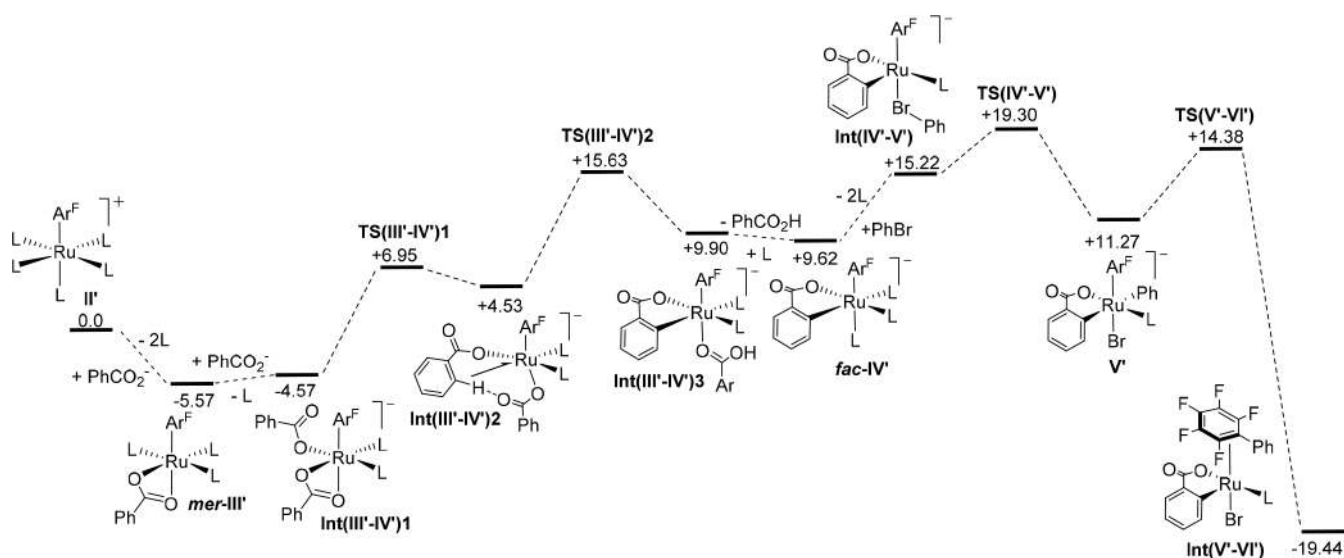


Figure 5. Jaffé plots displaying a linear free energy relationship between the benzoate source and the reaction rate ( $\rho_m \cong 2.2$ ;  $\rho_p \cong -1.2$ ).



**Figure 6.** Computed free energy reaction profile ( $\omega$ B97X-D(BS2, acetonitrile)//BP86, L = MeCN, Ar<sup>F</sup> = C<sub>6</sub>F<sub>5</sub>, kcal/mol) for the arylation of C<sub>6</sub>F<sub>5</sub>H with PhBr starting from model intermediate [Ru(C<sub>6</sub>F<sub>5</sub>)(MeCN)<sub>5</sub>]<sup>+</sup>, II'.

and by *meta*-EWGs, which is consistent with the observation that OMe and OEt substituents are visibly outliers in both V-shaped Hammett plots. Importantly, as the *meta* effect is more significant than the *para* one, it should also be noted that in the *para* V-shaped Hammett plot both OPh and F significantly deviate from linearity, as both rates are largely underestimated due to the greater contribution of the *meta* effect. Instead in the *meta* V-shaped Hammett plot OPh and F are marginally under- and overestimated, respectively. Although both substituents have positive  $\sigma_m$  (F = 0.34, OPh = 0.25), OPh has a slightly negative  $\sigma_p$  (-0.03), while F has a slightly positive one (0.06), which explains why OPh lies above and F below the linear fitting.

Jaffé equation:

$$\frac{\log\left(\frac{k_X}{k_H}\right)}{\sigma_m} = \frac{\rho_p \sigma_p}{\sigma_m} + \rho_m \quad (2)$$

Jaffé equation:

$$\frac{\log\left(\frac{k_X}{k_H}\right)}{\sigma_p} = \frac{\rho_m \sigma_m}{\sigma_p} + \rho_p \quad (3)$$

**2.4. DFT Studies.** We have also probed the mechanism of these benzoate-assisted arylation reactions with density functional theory (DFT) calculations. The reaction of a model system, [Ru(C<sub>6</sub>F<sub>5</sub>)(MeCN)<sub>5</sub>]<sup>+</sup> (denoted II'), with PhBr in the presence of PhCO<sub>2</sub><sup>-</sup> was considered, with all geometries optimized with the BP86 functional using a modest basis set (BS1, see Computational Details, SI, section 9). Energies were then recomputed using the  $\omega$ B97X-D functional with a def2-TZVP basis set and incorporating MeCN solvation via a PCM correction. Test calculations indicated the use of MeCN in place of the *t*-BuCN ligands had little effect on the overall profile, with most stationary points being destabilized by 2–4 kcal/mol (see Figure S21). Figure 6 summarizes the most accessible computed free energy profile based on the proposed catalytic cycle in Scheme 2. For each step alternative geometric isomers were assessed and details are supplied in the

SI (Figures S3–S7). Intermediates involved in ligand exchange steps are omitted here for clarity but are considered in the kinetic modeling (see below, Figure 9a). Starting with [Ru(C<sub>6</sub>F<sub>5</sub>)(MeCN)<sub>5</sub>]<sup>+</sup>, II', exchange of two MeCN ligands with PhCO<sub>2</sub><sup>-</sup> yields *mer*-[Ru(C<sub>6</sub>F<sub>5</sub>)(MeCN)<sub>3</sub>( $\kappa^2$ -PhCO<sub>2</sub>)], *mer*-III', which at -5.57 kcal/mol proves to be the most stable intermediate prior to the C–H and C–Br bond activation events. Further MeCN/PhCO<sub>2</sub><sup>-</sup> substitution forms [Ru(C<sub>6</sub>F<sub>5</sub>)(MeCN)<sub>2</sub>( $\kappa^1$ -PhCO<sub>2</sub>)( $\kappa^2$ -PhCO<sub>2</sub>)], Int(III'–IV')1 at -4.57 kcal/mol. This species then undergoes a 2-step C–H activation via agostic intermediate Int(III'–IV')2 at +4.53 kcal/mol from which C–H bond cleavage proceeds via an AMLA-6/CMD (ambiphilic metal–ligand assistance/concerted metalation deprotonation) transition state,<sup>18</sup> TS(III'–IV')2, at +15.63 kcal/mol (see also Figure 7 for

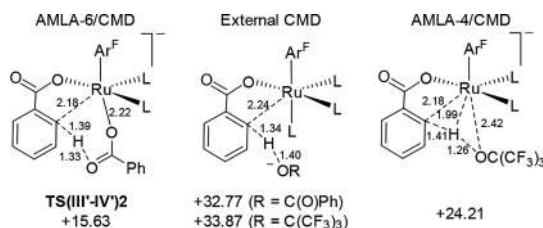


**Figure 7.** Geometries of alternative C–H activation transition states with selected key distances in Å and relative free energies in kcal/mol (L = MeCN, Ar<sup>F</sup> = C<sub>6</sub>F<sub>5</sub>). Geometric data for the external CMD transition state are for R = C(O)Ph; see SI for more details and alternative isomers (Figures S8 and S9).

geometric details). This gives a cyclometalated species Int(III'–IV')3 at +9.90 kcal/mol as a benzoic acid adduct. PhCO<sub>2</sub>H/MeCN substitution then forms *fac*-IV' at +9.62 kcal/mol.<sup>19</sup> The overall barrier to C–H activation is 21.20 kcal/mol, and the formation of *fac*-IV' is endergonic by 15.19 kcal/mol.

Alternative C–H bond activation mechanisms were also assessed and shown to be energetically less accessible (Figure 7 and Figure S8 and S9). Thus, transition states for external CMD at [Ru(C<sub>6</sub>F<sub>5</sub>)(MeCN)<sub>3</sub>( $\kappa^1$ -PhCO<sub>2</sub>)] by PhCO<sub>2</sub><sup>-</sup> lie above 30 kcal/mol. A direct role for <sup>-</sup>OC(CF<sub>3</sub>)<sub>3</sub> as a base in

C–H activation was also ruled out, either as an external CMD process or as an intramolecular base (AMLA-4/CMD). We return to the role of  $\text{OC}(\text{CF}_3)_3$  in promoting the arylation reaction below.

PhBr activation at *fac-IV'* requires initial MeCN substitution and, in principle, could occur at 6-coordinate  $[\text{Ru}(\text{C}_6\text{F}_5)(\text{MeCN})_2(\kappa\text{-C},\text{O}-\text{C}_6\text{H}_4\text{CO}_2)(\text{PhBr})]^-$ , either as a concerted oxidative addition to yield  $18e^-$  Ru(IV)  $[\text{Ru}(\text{C}_6\text{F}_5)(\text{MeCN})_2(\kappa\text{-C},\text{O}-\text{C}_6\text{H}_4\text{CO}_2)(\text{Ph})(\text{Br})]^-$  or via nucleophilic displacement of  $\text{Br}^-$  to form  $16e^-$   $\text{Ru}(\text{C}_6\text{F}_5)(\text{MeCN})_2(\kappa\text{-C},\text{O}-\text{C}_6\text{H}_4\text{CO}_2)(\text{Ph})$  (see Figure 8 and Figures S10 and S11).

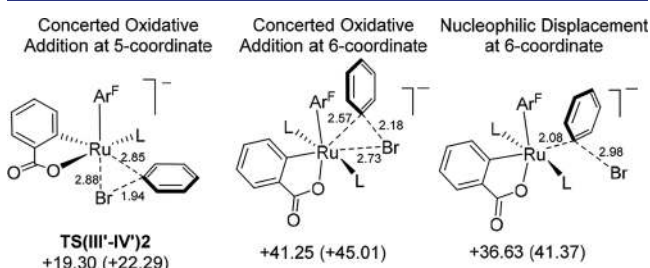


**Figure 8.** Geometries of alternative C–Br activation transition states with selected key distances in Å and relative free energies in kcal/mol ( $L = \text{MeCN}$ ,  $\text{Ar}^F = \text{C}_6\text{F}_5$ ). Examples shown are the lowest energy transition states located for each process; full details of isomers are in the SI (Figures S10 and S11). Data in parentheses are those where the PCM correction for acetonitrile solvent is included in the optimization procedure.

Such processes, however, proved to have very large barriers. Instead a second MeCN ligand is lost to form square-pyramidal  $[\text{Ru}(\text{C}_6\text{F}_5)(\text{MeCN})(\kappa\text{-C},\text{O}-\text{C}_6\text{H}_4\text{CO}_2)(\kappa\text{-Br-PhBr})]^-$ , *Int(IV'–V')*. This species has 12 possible geometric isomers of which 11 proved to be local minima (see Figure S7); the lowest energy form is shown in Figure 6 and benefits from having the strong donor aryl ligand in the axial position as well as the weak PhBr ligand opposite the high *trans* influence  $\text{C}_6\text{F}_5$ . PhBr is computed to prefer binding through the Br substituent over alternative  $\eta^2\text{-C}_6\text{H}_5\text{Br}$  forms, and IRC calculations subsequently confirmed that this Br-bound intermediate lies directly on the pathway for concerted oxidative addition. This proceeds via *TS(IV'–V')* at 19.30 kcal/mol to give *V'* at +11.27 kcal/mol. Ph– $\text{C}_6\text{F}_5$  reductive coupling then readily occurs via *TS(V'–VI')* at +14.38 kcal/mol and gives *Int(V'–VI')* (–19.44 kcal/mol) in which the biaryl product is bound in an  $\eta^2$ -fashion to Ru.<sup>20</sup> The free energy profile for arylation in Figure 6 indicates that the overall rate-limiting process is associated with C–Br activation via *TS(IV'–V')* at +19.30 kcal/mol and that this corresponds to an overall barrier of 24.87 kcal/mol. C–H activation is therefore a pre-equilibrium, the endergonic nature of which is consistent with reversible C–H activation leading to H/D exchange at the *ortho* position and a modest (equilibrium) kinetic isotope effect.

As discussed above and shown in Figure 7, the role of the  $\text{OC}(\text{CF}_3)_3$  additive in promoting arylation cannot be ascribed to any direct participation in the C–H activation event. Instead we postulate that  $\text{OC}(\text{CF}_3)_3$  affects the position of the C–H activation pre-equilibrium via deprotonation of the benzoic acid produced in this process. Based on the  $\text{p}K_a$  values of  $\text{PhCO}_2\text{H}$  and  $\text{HOC}(\text{CF}_3)_3$  in water (4.2 and 5.2, respectively) this implies a free energy change of –1.4 kcal/mol upon deprotonation. To quantify this effect, a kinetic

model accommodating all the steps linking *II'* to *Int(V'–VI')* was constructed (see Figure 9a) where any ligand substitution processes were treated as dissociative in nature with the ligand addition steps assumed to occur at the diffusion-controlled limit ( $k = 10^{10} \text{ M}^{-1} \text{ s}^{-1}$ , corresponding to a barrier of 4.78 kcal/mol at 363 K). This allows for the rate of the related ligand dissociation to be defined, based on the equilibrium constant computed for the overall ligand exchange. Within this model  $\text{OC}(\text{CF}_3)_3$  intervenes upon loss of  $\text{PhCO}_2\text{H}$  from species I, and its effect is modeled by a 1.4 kcal/mol stabilization of all species from J onward (right-hand shaded area, Figure 9b). This leaves the rates of the onward reactions unchanged but reduces the rate of the backward reaction (i.e.,  $\text{J} + \text{PhCO}_2\text{H} \rightarrow \text{I}$ ). The effect is seen in Figure 9c, plot i, which shows that product formation (modeled by species N) is approximately doubled over a 1 h period in the presence of the  $\text{OC}(\text{CF}_3)_3$  additive (compare the dotted and solid red lines). This is in good agreement with experimental observations, which indicate a ca. 3-fold rate enhancement (Figure 1).

The profile in Figure 9b was recomputed with two substituted benzoates,  $4\text{-R-C}_6\text{H}_4\text{CO}_2^-$ , with  $\text{R} = \text{NMe}_2$  and  $\text{CF}_3$ . These substituents have distinctly different  $\sigma_p$  and  $\sigma_m$  Hammett parameters, yet experimentally both provide significantly enhanced reactivity compared to the parent benzoate (Table 1). In each case, a similar overall profile was computed, with the transition state for C–Br activation lying above that for C–H activation (see Table 2 and Figures S12 and S13). The results again emphasize the sensitivity of the overall outcome to the inclusion of the  $\text{OC}(\text{CF}_3)_3$  additive in the model. This is more apparent for  $4\text{-CF}_3\text{-C}_6\text{H}_4\text{CO}_2^-$  for which a reduction of 2.16 kcal/mol in  $\Delta G_{\text{CHA}}$  leads to an order of magnitude reduction in the computed  $t_{1/2}$ , the time required to reach 50% conversion. The higher  $\text{p}K_a$  of  $4\text{-NMe}_2\text{-C}_6\text{H}_4\text{CO}_2\text{H}$  means the effect here is less dramatic, but in this case, the computed barrier in the absence of  $\text{OC}(\text{CF}_3)_3$  is already significantly lower than the  $\text{PhCO}_2^-/\text{OC}(\text{CF}_3)_3$  system.

The data in Table 2 indicate that the overall barrier to arylation ( $\Delta G_{\text{span}}^\ddagger$ ) depends more on the free energy change of the C–H activation ( $\Delta G_{\text{CHA}}$ ) rather than the subsequent barrier to PhBr activation ( $\Delta G_{\text{PhBr}}^\ddagger$ ). The variation in  $\Delta G_{\text{CHA}}$  is mirrored in the trend in the 2-step C–H activation ( $\text{G} \rightarrow \text{I}$ :  $\text{R} = \text{NMe}_2$  (+12.23 kcal/mol) <  $\text{R} = \text{CF}_3$  (+13.74 kcal/mol) <  $\text{R} = \text{H}$  (14.47 kcal/mol)). The fact that both an electron-donating and an electron-withdrawing substituent reduce the barrier to C–H activation over the unsubstituted parent has parallels in the trends computed by Gorelsky and Fagnou for C–H activation of (hetero)aromatics at  $\text{Pd}(\text{Ph})(\text{OAc})(\text{PMe}_3)$ ,<sup>4d,22</sup> although the variations are much smaller here. The effect of the  $\text{OC}(\text{CF}_3)_3$  base is also a significant factor in accelerating the reaction, especially with the  $4\text{-CF}_3\text{-C}_6\text{H}_4\text{CO}_2^-$  additive.

As highlighted in Figure 4, electronic perturbation arising from the benzoate substituent, R, could manifest itself at several points along the reaction pathway. The initial cyclometalation involves  $\text{C}_{\text{Ar}}\text{–H}$  bond cleavage and formation of a  $\text{C}_{\text{Ar}}\text{–}[\text{Ru}]$  bond, both of which should be sensitive to  $\sigma_m$ ; similarly this process involves varying the  $\text{C}(\text{O})\text{O}\text{–}[\text{Ru}]$  interaction and  $\text{H}^+$  transfer to a second benzoate to form a  $\text{C}(\text{O})\text{O}\text{–H}$  bond, which will be more dependent on  $\sigma_p$ . As discussed above, the C–Br activation step shows little dependence on R, so we have focused on deconvoluting how  $\sigma_m$  and  $\sigma_p$  affect  $\Delta G_{\text{CHA}}$ .



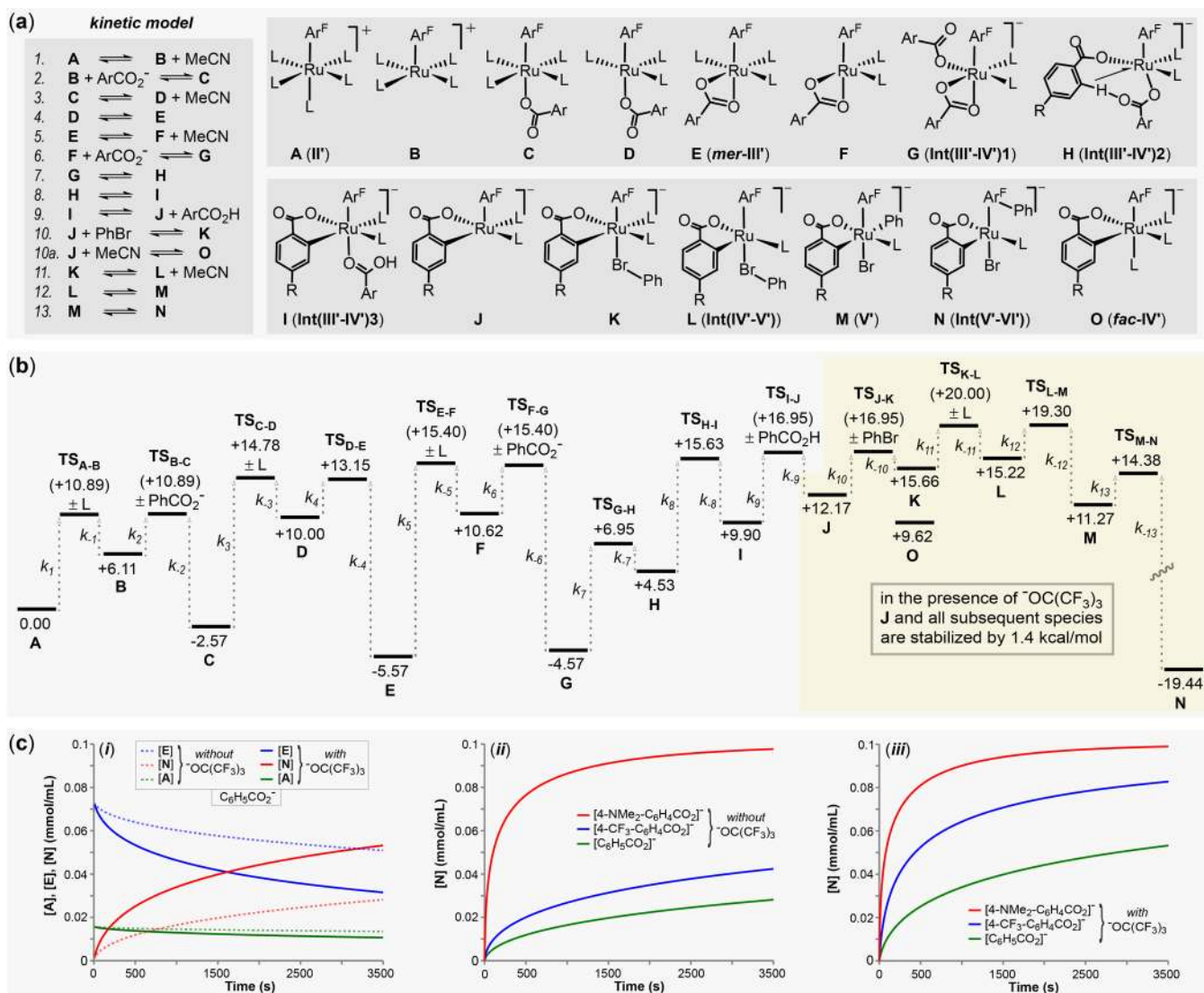
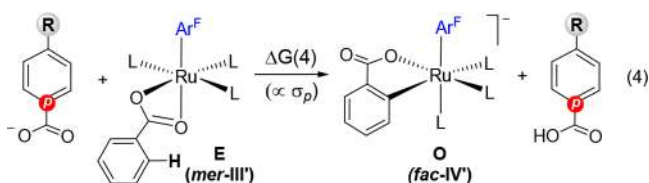
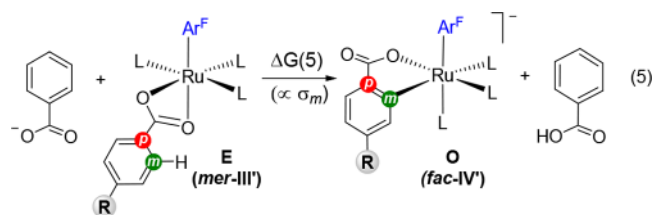


**Figure 9.** (a) Kinetic model for the reaction of  $\text{II}'$  (denoted A in the kinetic model) with PhBr in the presence of benzoates 4-R-C<sub>6</sub>H<sub>4</sub>CO<sub>2</sub><sup>-</sup> to give  $\text{Int}(\text{V}'\text{-VI}')$  (denoted N; L = MeCN, Ar<sup>F</sup> = C<sub>6</sub>F<sub>5</sub>). Ligand addition steps are assumed to proceed at the diffusion-controlled limit and are indicated by TS energies shown in parentheses. (b) Computed reaction profile (kcal/mol) with PhCO<sub>2</sub><sup>-</sup> highlighting the effect of the  ${}^-\text{OC}(\text{CF}_3)_3$  additive; see Figures S12 and S13 for equivalent diagrams computed with 4-NMe<sub>2</sub>-C<sub>6</sub>H<sub>4</sub>CO<sub>2</sub><sup>-</sup> and 4-CF<sub>3</sub>-C<sub>6</sub>H<sub>4</sub>CO<sub>2</sub><sup>-</sup>. (c) Computed kinetic profiles at 363 K comparing arylation (i) in the presence of PhCO<sub>2</sub><sup>-</sup>, with and without the  ${}^-\text{OC}(\text{CF}_3)_3$  additive, (ii) in the presence of benzoates 4-R-C<sub>6</sub>H<sub>4</sub>CO<sub>2</sub><sup>-</sup> (R = H, NMe<sub>2</sub> and CF<sub>3</sub>) without  ${}^-\text{OC}(\text{CF}_3)_3$ , and (iii) in the presence of benzoates 4-R-C<sub>6</sub>H<sub>4</sub>CO<sub>2</sub><sup>-</sup> (R = H, NMe<sub>2</sub> and CF<sub>3</sub>) with added  ${}^-\text{OC}(\text{CF}_3)_3$ .

To this end, we have computed the free energy changes for the model cyclometalation processes (eqs 4 and 5) for all the



4-R-C<sub>6</sub>H<sub>4</sub>CO<sub>2</sub><sup>-</sup> substrates studied experimentally (see Figure 10 and Table S5). In eq 4 cyclometalation of the parent benzoate in E proceeds with different 4-R-C<sub>6</sub>H<sub>4</sub>CO<sub>2</sub><sup>-</sup> acting as the base:  $\Delta G(4)$  should therefore reflect how  $\sigma_p$  promotes C-H activation. In eq 5, the cyclometalation of different 4-R-C<sub>6</sub>H<sub>4</sub>CO<sub>2</sub><sup>-</sup> in E proceeds with the parent benzoate acting as the base.  $\Delta G(5)$  should be dominated by the breaking of the



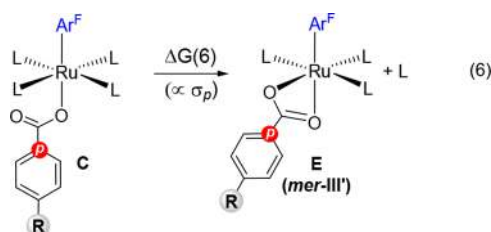
C<sub>Ar</sub>-H bond and the formation of the new [Ru]-C<sub>Ar</sub> bond and, as such, should correlate with  $\sigma_m$ . However,  $\sigma_p$  may also play a role here by influencing how the C(O)O-[Ru] interaction varies due to the  $\kappa^2\text{-}\kappa^1$  change in substrate binding mode. This point was considered in process 6 and was found to be favored by electron-donating *para*-substituents. This effect is relatively weak, however, with a plot of  $\Delta G(6)$  vs  $\sigma_p$  giving a straight line of gradient 2.1 ( $R^2 = 0.92$ , see Graph S9).

**Table 2. Selected Computed Data (kcal/mol unless otherwise stated) for the Arylation Reaction with Different Benzoates 4-R-C<sub>6</sub>H<sub>4</sub>CO<sub>2</sub><sup>-a,b</sup>**

R	<sup>-</sup> OC(CF <sub>3</sub> ) <sub>3</sub>	$\Delta G_{\text{CHA}}^{\ddagger}$	$\Delta G_{\text{CHA}}$	$\Delta G_{\text{PhBr}}^{\ddagger}$	$\Delta G_{\text{span}}^{\ddagger}$	$t_{1/2}$ (s)
H	N	21.20	+17.74	7.13	24.87	18102
	Y		+16.34		23.40	2954
NMe <sub>2</sub>	N	19.77	+13.93	7.32	21.25	106
	Y		+13.65		20.97	81
CF <sub>3</sub>	N	19.84	+16.15	7.61	23.76	6084
	Y		+13.99		21.60	446

<sup>a</sup>Definitions:  $\Delta G_{\text{CHA}}^{\ddagger} = \Delta G(\text{TS}_{\text{H-I}} - \text{E})$ ;  $\Delta G_{\text{CHA}} = \Delta G(\text{J} - \text{E})$ ;  $\Delta G_{\text{PhBr}}^{\ddagger} = \Delta G(\text{TS}_{\text{L-M}} - \text{J})$ ;  $\Delta G_{\text{span}}^{\ddagger} = \Delta G(\text{TS}_{\text{L-M}} - \text{E})$ ;<sup>21</sup>  $t_{1/2}$  = time to 50% conversion. See Figure 9 for labels of stationary points.

<sup>b</sup>Corrections for the effect of <sup>-</sup>OC(CF<sub>3</sub>)<sub>3</sub> are based on the pK<sub>a</sub> values of HOC(CF<sub>3</sub>)<sub>3</sub> (5.2) and PhCO<sub>2</sub>H (4.2) in water; pK<sub>a</sub> values for the 4-R-C<sub>6</sub>H<sub>4</sub>CO<sub>2</sub>H acids (R = NMe<sub>2</sub>, 5.03; R = CF<sub>3</sub>, 3.66) are based on the difference in the  $\sigma_p$  Hammett parameters and the relationship  $\sigma = -(\text{pK}_a(4\text{-R-C}_6\text{H}_4\text{CO}_2\text{H}) - \text{pK}_a(\text{PhCO}_2\text{H}))$ .



Plots of  $\Delta G(4)$  versus  $\sigma_p$  and  $\Delta G(5)$  versus  $\sigma_m$  are displayed in Figure 10. In both cases, a good correlation is found; moreover, the plots provide further evidence for the counterbalancing effects of the *para*- and *meta*-substituents. Thus, the cyclometalation is facilitated by electron-donating *para*-substituents, which enhance substrate basicity ( $\Delta G(4)$  versus  $\sigma_p$ ), while for a given base substrate, cyclometalation is favored by electron-withdrawing *meta*-substituents ( $\Delta G(5)$  versus  $\sigma_m$ ).<sup>23</sup> Importantly, the gradients indicate the latter *meta* effect is approximately twice as large as the former *para* effect, in excellent agreement with the conclusions from the Jaffé plots in Figure 5.

The trend in the *meta* effect as defined in eq 5 must relate to differences in the C<sub>Ar</sub>-H and [Ru]-C<sub>Ar</sub> bond energies. Direct computation of the C<sub>Ar</sub>-H homolytic bond dissociation energies shows little variation as a function of R, with most benzoates giving a value of 102 ± 0.5 kcal/mol (see SI, Table

S6). The [Ru]-C<sub>Ar</sub> bond strength must therefore dominate, with these being stronger with electron-withdrawing substituents. There is precedent for this in the selective C-H activation of fluoroarenes<sup>24</sup> and in M-C bond strengths being more sensitive to substituent effects than their equivalent C-H bonds.<sup>25</sup>

**2.5. The Role of Benzoate Cyclometalation in Promoting Arylation.** Although the C-Br activation step proved insensitive to substituent effects on the benzoate, cyclometalation remains the key to making the overall arylation process accessible. To understand this more fully, C-Br activation was modeled at cationic, neutral, and non-cyclometalated anionic analogues of L/Int(IV'-V'), and the most accessible processes for each case are shown in Figure 11. The data show two trends when moving from cationic through neutral and then to anionic systems: (i) the 5-coordinate precursor to C-Br activation becomes more accessible and (ii) the subsequent barrier to C-Br activation is reduced. Both factors make the overall barriers at [Ru(C<sub>6</sub>F<sub>5</sub>)(MeCN)<sub>2</sub>(κ<sup>2</sup>-PhCO<sub>2</sub>)(PhBr)] prohibitively high. This is still the case for [Ru(C<sub>6</sub>F<sub>5</sub>)(MeCN)(κ<sup>1</sup>-PhCO<sub>2</sub>)<sub>2</sub>(PhBr)]<sup>-</sup>,<sup>26</sup> although interestingly for [Ru(C<sub>6</sub>F<sub>5</sub>)(κ<sup>2</sup>-PhCO<sub>2</sub>)(κ<sup>1</sup>-PhCO<sub>2</sub>)<sub>2</sub>(PhBr)]<sup>-</sup> the barrier to C-Br activation falls to only 3.97 kcal/mol. This is in fact slightly lower than the barrier from cyclometalated L (4.08 kcal/mol), although in this case the low energy of L (+15.22 kcal/mol) allows C-Br activation to proceed via TS<sub>L-M</sub>/TS(IV'-V') at only +19.30 kcal/mol. The role of the cyclometalated benzoate is therefore not just to enhance the electron-rich character of the Ru(II) center but also to facilitate ligand dissociation and thus render the 5-coordinate precursor to C-Br activation accessible. The high *trans* influence of the cyclometalated arm is therefore a key factor in promoting reactivity.

The cyclometalated benzoate ligand also plays an important role in dictating the selectivity of the C-C coupling process. The computed structures of the 6-coordinate Ru(IV) species such as intermediate M formed upon C-Br activation show a marked distortion away from an octahedral geometry, with a narrowing of the *trans*-C1-Ru-C2 bond that pushes one of the dπ orbitals up in energy (see Figure 12).<sup>27</sup> This distortion will tend to favor a low spin d<sup>4</sup> configuration, whereas geometries computed in the triplet state (which are often energetically competitive for these Ru(IV) species<sup>28</sup>) exhibit more regular pseudo-octahedral structures.

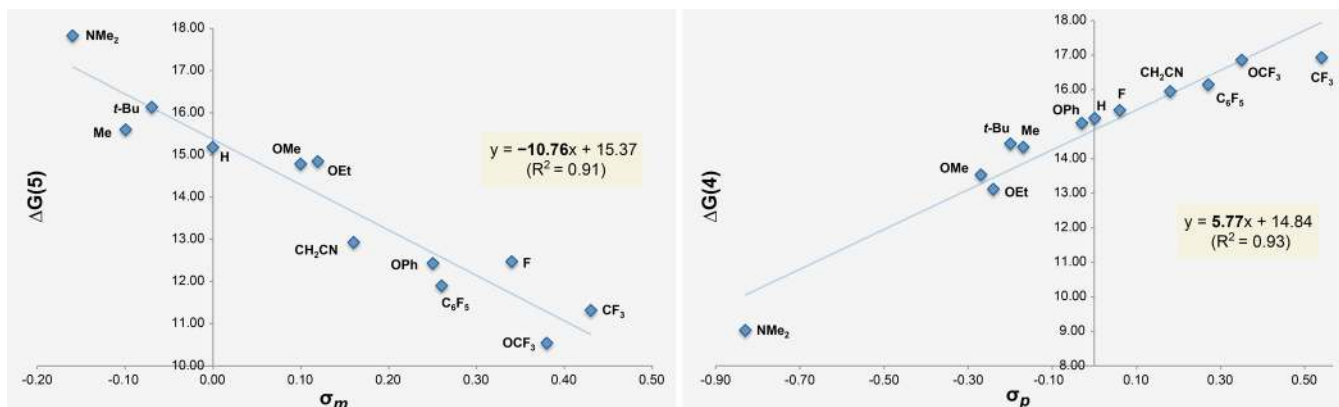


**Figure 10.** Model reactions considered to isolate  $\sigma_p$  and  $\sigma_m$  effects and the resultant plots of  $\Delta G(4)$  vs  $\sigma_p$  and  $\Delta G(5)$  vs  $\sigma_m$ .



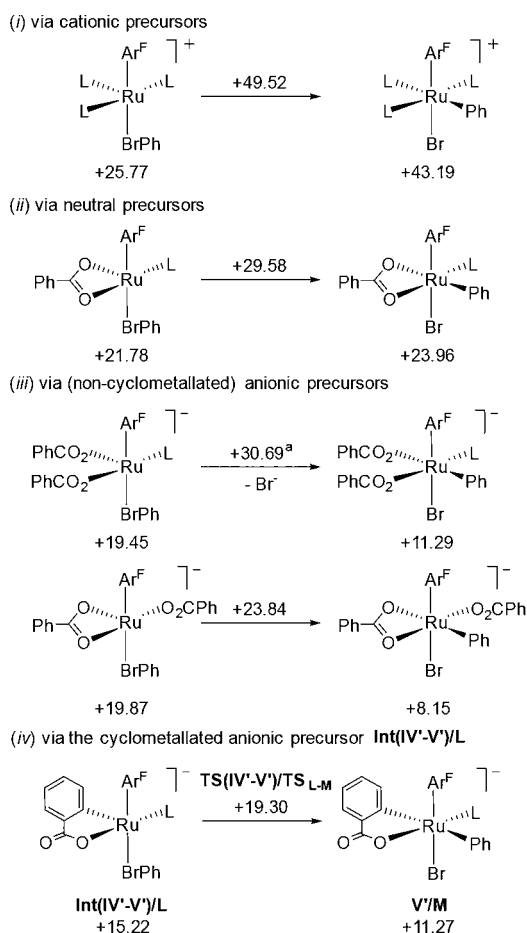


**Figure 11.** Lowest energy pathways (kcal/mol, L = MeCN, Ar<sup>F</sup> = C<sub>6</sub>F<sub>5</sub>) computed for C–Br activation at 5-coordinate cationic, neutral, and anionic precursors, placing the Ph group *cis* to C<sub>6</sub>F<sub>5</sub>.<sup>a</sup> Proceeds via nucleophilic displacement of Br<sup>−</sup>; all other pathways involve a concerted oxidative addition. See Figures S15–S19 for details and alternative pathways.

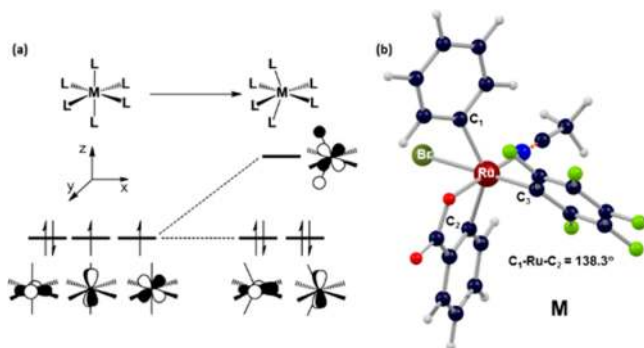


**Figure 12.** (a) Changes in the relative energies of the metal-based  $d\pi$  orbitals and preferred spin state upon narrowing one *trans*-L–M–L angle in  $d^4$   $\text{ML}_6$  complexes. (b) Computed geometry of intermediate **M** highlighting the reduced *trans*-C<sub>1</sub>–Ru–C<sub>2</sub> angle.

Distortion of the singlet is most favorable when strong  $\sigma$ -donors adopt a mutually *trans* arrangement, so the most stable isomers of Ru(IV) species **M** feature the three strongly donating aryl ligands in a *mer* configuration. One of these, **M(ii)**, has Ph *trans* to C<sub>6</sub>F<sub>5</sub> and is actually more stable than **M** itself (see Figure 13); moreover C–C coupling with the benzoate ligand in **M(ii)** proceeds through a lower transition

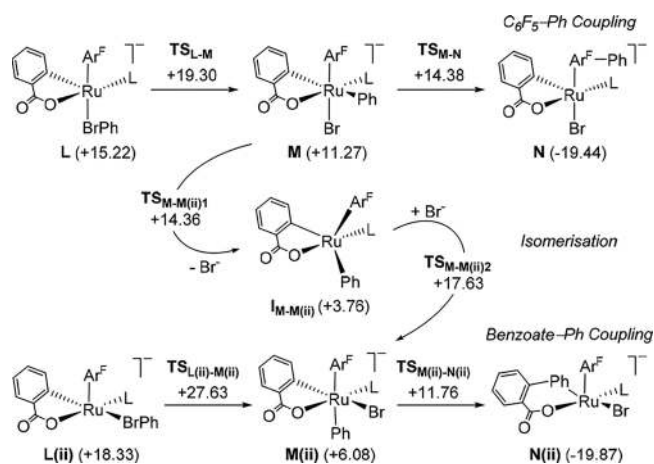


**Figure 13.** Key stationary points (kcal/mol) for the competition between C<sub>6</sub>F<sub>5</sub>–Ph coupling via intermediate **M** and benzoate–Ph coupling via intermediate **M(ii)** (L = MeCN, Ar<sup>F</sup> = C<sub>6</sub>F<sub>5</sub>).

state,  $\text{TS}_{\text{M(ii)-N(ii)}} (+11.76 \text{ kcal/mol})$ , than that for Ph–C<sub>6</sub>F<sub>5</sub> coupling via  $\text{TS}_{\text{M-N}} (+14.38 \text{ kcal/mol})$ . The fact that benzoate–Ph coupling is *not* observed is due to **M(ii)** being kinetically inaccessible, either through C–Br activation at **L(ii)** (via  $\text{TS}_{\text{L(ii)-M(ii)}} (+27.63 \text{ kcal/mol})$ ) or through isomerization of **M**. The lowest energy isomerization pathway involves Br<sup>−</sup> loss to form the neutral trigonal bipyramidal intermediate  $\text{I}_{\text{M-M(ii)}}$  followed by Br<sup>−</sup> reassociation to give **M(ii)**; this second step involves transition state  $\text{TS}_{\text{M-M(ii)2}}$ , which at 17.63 kcal/mol is >3 kcal/mol higher than  $\text{TS}_{\text{M-N}}$  at 14.38 kcal/mol. Benzoate–C<sub>6</sub>F<sub>5</sub> coupling from either **M** or **M(ii)** is also significantly less accessible (see Figure S20). More generally, for the systems in Figure 11 that lack a cyclometalated ligand, C–Br activation is computed to be more accessible when the Ph ligand moves *trans* to C<sub>6</sub>F<sub>5</sub>. The presence of the cyclometalated benzoate therefore promotes the formation of a Ru(IV) intermediate where the Ph and C<sub>6</sub>F<sub>5</sub> can be mutually *cis*, thus facilitating the observed selectivity of the subsequent C–C coupling.

The computed data highlight how a C–H functionalization process can be promoted through use of a base additive such as (NMe<sub>4</sub>)OC(CF<sub>3</sub>)<sub>3</sub> and how a subtle perturbation of a C–H activation pre-equilibrium step can have a significant effect on the overall reaction efficiency. Group 1 carbonate salts, M<sub>2</sub>CO<sub>3</sub>, have often been proposed as proton sinks in direct arylation reactions,<sup>29</sup> and the choice of the Group 1 M<sup>+</sup> cation can significantly impact the end result when expressed as a reaction yield. The results here highlight how such variations can result from small changes in the efficiency of these processes that could reflect, for example, changes in additive concentration due to varying solubilities in organic reaction media.

### 3. CONCLUSIONS

A detailed experimental and *in silico* mechanistic investigation allowed the elucidation of the role of the benzoate salt in promoting aryl halide oxidative addition in the Ru(II)-catalyzed C–H arylation of fluoroarenes. The inability of 2,6-disubstituted benzoate sources to trigger the desired arylation event, along with D/H scrambling and kinetic isotope effect experiments, supported the hypothesis for the requirement of a cyclometalation step of the benzoate salt. Thus, the resulting highly electron-rich anionic Ru(II) intermediate rapidly undergoes oxidative addition with the

aryl halide to furnish the biaryl product via a selective reductive elimination step. The pre-equilibrium associated with the kinetically relevant benzoate cyclometalation leads to a Jaffé relationship reflecting the influence of the benzoate substituents at multiple distinctive sites in this process. Indeed, simple Hammett plots correlating the electronic perturbation at only one reactive site at the time could not provide a linear free energy relationship that accommodated all the substituents studied.

DFT calculations provide support for a mechanism involving reversible C–H activation and formation of an anionic cyclometalated intermediate. The enhanced lability of this species allows access to a reactive 5-coordinate intermediate capable of C–Br bond cleavage. A kinetic model based on the computed mechanism captures the rate enhancement observed with *p*-substituted benzoates bearing both electron withdrawing and electron donating substituents. The role of a (NMe<sub>4</sub>)OC(CF<sub>3</sub>)<sub>3</sub> additive in promoting reactivity is pinpointed to the deprotonation of the carboxylic acid formed upon cyclometalation that shifts the pre-equilibrium associated with benzoate cyclometalation. This effect is particularly marked for less basic benzoates such as (NMe<sub>4</sub>)(4-CF<sub>3</sub>-C<sub>6</sub>H<sub>4</sub>CO<sub>2</sub>), the conjugate acids of which will be more readily deprotonated by the (NMe<sub>4</sub>)OC(CF<sub>3</sub>)<sub>3</sub> additive. Both the experimental and computational results highlight the counterbalancing effects of electron-withdrawing groups *meta* to the site of benzoate cyclometalation and electron-donating groups *para* to the proton-accepting carboxylate group in promoting reactivity, with the former having the larger influence by a factor of approximately 2.

Finally, this mechanistic breakthrough has important implications on the design of new catalytic systems involving an oxidative addition at Ru(II) centers, which have been significantly underdeveloped due to the lack of knowledge surrounding this fundamental step.

## ■ ASSOCIATED CONTENT

### Supporting Information

The Supporting Information is available free of charge on the ACS Publications website at DOI: 10.1021/jacs.8b08150.

Experimental procedures and characterization data (PDF)

Computed Cartesian coordinates for all stationary points (XYZ)

## ■ AUTHOR INFORMATION

### Corresponding Authors

\*igor.larrosa@manchester.ac.uk

\*s.a.macgregor@hw.ac.uk

### ORCID

Stuart A. Macgregor: 0000-0003-3454-6776

Igor Larrosa: 0000-0002-5391-7424

### Notes

The authors declare no competing financial interest.

## ■ ACKNOWLEDGMENTS

We gratefully acknowledge the Engineering and Physical Sciences Research Council (EPSRC, EP/L014017/2) for funding and the European Research Council for a Starting Grant (to I.L.). We thank Prof. Eric Clot (Université de Montpellier) for valuable discussion regarding the kinetic

simulations, EU COST Action CM1205 – CARISMA for a Short-Term Scientific Mission award to R.K., and Heriot-Watt University for support.

## ■ REFERENCES

- (1) (a) Zahn, A.; Brotschi, C.; Leumann, C. *Chem. - Eur. J.* **2005**, *11*, 2125–2129. (b) DiMagno, S. G.; Sun, H. *Curr. Top. Med. Chem.* **2006**, *6*, 1473–1482. (c) Purser, S.; Moore, P. R.; Swallow, S.; Gouverneur, V. *Chem. Soc. Rev.* **2008**, *37*, 320–330. (d) Liang, T.; Neumann, C. N.; Ritter, T. *Angew. Chem., Int. Ed.* **2013**, *52*, 8214–8264. (e) Selby, T. P.; Bereznak, J. F.; Bisaha, J. J.; Ding, A. X.; Gopalsamuthiram, V.; Hanagan, M. A.; Long, J. K.; Taggi, A. E. Fungicidal substituted azoles. International Patent WO 2009137651 A8, 2009. (f) Gregory, V.; Taggi, A. E. Fungicidal Mixtures. International Patent WO 2011056463 A2, 2011. (g) Babudri, F.; Naso, F.; Ragni, R.; Farinola, G. M. *Chem. Commun.* **2007**, 1003–1022. (h) Tang, M. L.; Reichardt, A. D.; Miyaki, N.; Stoltenberg, R. M.; Bao, Z. *J. Am. Chem. Soc.* **2008**, *130*, 6064–6065. (i) Wang, Y.; Watson, M. D. *J. Am. Chem. Soc.* **2006**, *128*, 2536–2537. (j) Tsuzuki, T.; Shirasawa, N.; Suzuki, T.; Tokito, S. *Adv. Mater.* **2003**, *15*, 1455–1458. (k) Weck, M.; Dunn, A. R.; Matsumoto, K.; Coates, G. W.; Lobkovsky, E. B.; Grubbs, R. H. *Angew. Chem., Int. Ed.* **1999**, *38*, 2741–2745. (l) Nitschke, J. R.; Tilley, T. D. *J. Am. Chem. Soc.* **2001**, *123*, 10183–10190. (m) Kitamura, T.; Wada, Y.; Yanagida, S. *J. Fluorine Chem.* **2000**, *105*, 305–311. (n) Sakamoto, Y.; Suzuki, T.; Miura, A.; Fujikawa, H.; Tokito, S.; Taga, Y. *J. Am. Chem. Soc.* **2000**, *122*, 1832–1833.
- (2) (a) DePasquale, R. J.; Tamborski, C. *J. Org. Chem.* **1969**, *34*, 1736–1740. (b) Coe, P. L.; Pearl, G. M. *J. Organomet. Chem.* **1971**, *31*, 55–57. (c) Frohn, H.-J.; Adonin, N. Y.; Bardin, V. V.; Starichenko, V. F. *J. Fluorine Chem.* **2002**, *117*, 115–120. (d) Korenaga, T.; Kosaki, T.; Fukumura, R.; Ema, T.; Sakai, T. *Org. Lett.* **2005**, *7*, 4915–4917. (e) Shang, R.; Fu, Y.; Wang, Y.; Xu, Q.; Yu, H.-Z.; Liu, L. *Angew. Chem., Int. Ed.* **2009**, *48*, 9350–9354. (f) Shang, R.; Xu, Q.; Jiang, Y.-Y.; Wang, Y.; Liu, L. *Org. Lett.* **2010**, *12*, 1000–1003. (g) Kinzel, T.; Zhang, Y.; Buchwald, S. L. *J. Am. Chem. Soc.* **2010**, *132*, 14073–14075.
- (3) Representative reviews on C–H activation: (a) Alberico, D.; Scott, M. E.; Lautens, M. *Chem. Rev.* **2007**, *107*, 174–238. (b) Ackermann, L.; Vicente, R.; Kapdi, A. R. *Angew. Chem., Int. Ed.* **2009**, *48*, 9792–9826. (c) Gutekunst, W. R.; Baran, P. S. *Chem. Soc. Rev.* **2011**, *40*, 1976–1991. (d) Lyons, T. W.; Sanford, M. S. *Chem. Rev.* **2010**, *110*, 1147–1169. (e) Boorman, T. C.; Larrosa, I. *Chem. Soc. Rev.* **2011**, *40*, 1910–1925. (f) Wencel-Delord, J.; Droge, T.; Liu, F.; Glorius, F. *Chem. Soc. Rev.* **2011**, *40*, 4740–4761. (g) Arockiam, P. B.; Bruneau, C.; Dixneuf, P. H. *Chem. Rev.* **2012**, *112*, 5879–5918. (h) Engle, K. M.; Mei, T.-S.; Wasa, M.; Yu, J.-Q. *Acc. Chem. Res.* **2012**, *45*, 788–802. (i) Juliá-Hernández, F.; Simonetti, M.; Larrosa, I. *Angew. Chem., Int. Ed.* **2013**, *52*, 11458–11460. (j) Girard, S. A.; Knauber, T.; Li, C. *Angew. Chem., Int. Ed.* **2014**, *53*, 74–100. (k) Kakiuchi, F.; Kochi, T.; Murai, S. *Synlett* **2014**, *25*, 2390–2414. (l) Tani, S.; Uehara, T. N.; Yamaguchi, J.; Itami, K. *Chem. Sci.* **2014**, *5*, 123–135. (m) Zhang, X.-S.; Chen, K.; Shi, Z. *Chem. Sci.* **2014**, *5*, 2146–2159. (n) Yang, J. *Org. Biomol. Chem.* **2015**, *13*, 1930–1941. (o) Dey, A.; Agasti, S.; Maiti, D. *Org. Biomol. Chem.* **2016**, *14*, 5440–545. (p) Dey, A.; Maiti, S.; Maiti, D. *Chem. Commun.* **2016**, *52*, 12398–12414. (q) Simonetti, M.; Cannas, D. M.; Larrosa, I. In *Advances in Organometallic Chemistry*; Perez, P. J., Ed.; Elsevier: Amsterdam, 2017; Vol. 67, pp 299–399.
- (4) (a) Lafrance, M.; Rowley, C. N.; Woo, T. K.; Fagnou, K. *J. Am. Chem. Soc.* **2006**, *128*, 8754–8756. (b) Lafrance, M.; Shore, D.; Fagnou, K. *Org. Lett.* **2006**, *8*, 5097–5100. (c) René, O.; Fagnou, K. *Org. Lett.* **2010**, *12*, 2116–2119. (d) Gorelsky, S. I. *Coord. Chem. Rev.* **2013**, *257*, 153–164. (e) Wei, Y.; Kan, J.; Wang, M.; Su, W.; Hong, M. *Org. Lett.* **2009**, *11*, 3346–3349. (f) Wei, Y.; Su, W. *J. Am. Chem. Soc.* **2010**, *132*, 16377–16379. (g) Li, H.; Liu, J.; Sun, C.-L.; Li, B.-J.; Shi, Z. *Org. Lett.* **2011**, *13*, 276–279.

(5) (a) Do, H.-Q.; Daugulis, O. *J. Am. Chem. Soc.* **2008**, *130*, 1128–1129. (b) Do, H.-Q.; Khan, R. M. K.; Daugulis, O. *J. Am. Chem. Soc.* **2008**, *130*, 15185–15192. (c) Do, H.-Q.; Daugulis, O. *Chem. Commun.* **2009**, 6433–6435. (d) Do, H.-Q.; Daugulis, O. *J. Am. Chem. Soc.* **2009**, *131*, 17052–17053. (e) Do, H.-Q.; Daugulis, O. *J. Am. Chem. Soc.* **2011**, *133*, 13577–13586.

(6) (a) Lu, P.; Boorman, T. C.; Slawin, A. M. Z.; Larrosa, I. *J. Am. Chem. Soc.* **2010**, *132*, 5580–5581. (b) Ahlsten, N.; Perry, G. J. P.; Cambeiro, X. C.; Boorman, T. C.; Larrosa, I. *Catal. Sci. Technol.* **2013**, *3*, 2892–2897. (c) Cambeiro, X. C.; Boorman, T. C.; Lu, P.; Larrosa, I. *Angew. Chem., Int. Ed.* **2013**, *52*, 1781–1784. (d) Cambeiro, X. C.; Ahlsten, N.; Larrosa, I. *J. Am. Chem. Soc.* **2015**, *137*, 15636–15639.

(7) Simonetti, M.; Perry, G. J. P.; Cambeiro, X. C.; Juliá-Hernández, F.; Arokianathar, J. N.; Larrosa, I. *J. Am. Chem. Soc.* **2016**, *138*, 3596–3606.

(8) Simonetti, M.; Cannas, D. M.; Just-Baringo, X.; Vitorica-Yrezabal, I. J.; Larrosa, I. *Nat. Chem.* **2018**, *10*, 724–731.

(9) (a) Ackermann, L. *Acc. Chem. Res.* **2014**, *47*, 281–295. (b) De Sarkar, S.; Liu, W.; Kozhushkov, S. I.; Ackermann, L. *Adv. Synth. Catal.* **2014**, *356*, 1461–1479. (c) Simonetti, M.; Larrosa, I. *Nat. Chem.* **2016**, *8*, 1086–1088.

(10) (a) Simonetti, M.; Cannas, D. M.; Panigrahi, A.; Kujawa, S.; Kryjewski, M.; Xie, P.; Larrosa, I. *Chem. - Eur. J.* **2017**, *23*, 549–553. (b) Huang, L.; Weix, D. J. *Org. Lett.* **2016**, *18*, 5432–5435. (c) Biafora, A.; Krause, T.; Hackenberger, D.; Belitz, F.; Gooßen, L. *J. Angew. Chem., Int. Ed.* **2016**, *55*, 14752–14755. (d) Mei, R.; Zhu, C.; Ackermann, L. *Chem. Commun.* **2016**, *52*, 13171–13174.

(11) (a) Ackermann, L. *Acc. Chem. Res.* **2014**, *47*, 281–295. (b) Ackermann, L.; Vicente, R.; Althammer, A. *Org. Lett.* **2008**, *10*, 2299–2302. (c) Ackermann, L.; Vicente, R.; Potukuchi, H. K.; Pirovano, V. *Org. Lett.* **2010**, *12*, 5032–5035. Ackermann, L. *Chem. Rev.* **2011**, *111*, 1315–1345. (e) Ferrer Flegeau, E.; Bruneau, C.; Dixneuf, P. H.; Jutand, A. *J. Am. Chem. Soc.* **2011**, *133*, 10161–10170.

(12) When (2,6-Me-C<sub>6</sub>H<sub>3</sub>CO<sub>2</sub>)(NMe<sub>4</sub>), (2,6-F-C<sub>6</sub>H<sub>3</sub>CO<sub>2</sub>)(NMe<sub>4</sub>), and (2,6-OMe-C<sub>6</sub>H<sub>3</sub>CO<sub>2</sub>)(NMe<sub>4</sub>) were tested in the presence of added (NMe<sub>4</sub>)OC(CF<sub>3</sub>)<sub>3</sub>, no cross-coupled product was detected.

(13) In light of the reversibility of steps I–IV (Scheme 3), the observed KIE of 1.36 could also be associated with the C–H activation step of C<sub>6</sub>F<sub>5</sub>H/D, which may be generated *in situ* via proto/deuterodemetalation of Ru1c with concomitant release of Ru(C<sub>6</sub>H<sub>5</sub>CO<sub>2</sub>)<sub>x</sub>(*t*-BuCN)<sub>y</sub> species. In order to rule this hypothesis out, we preincubated C<sub>6</sub>F<sub>5</sub>H (1 equiv), [Ru(*t*-BuCN)<sub>2</sub>](BF<sub>4</sub>)<sub>2</sub> (1 equiv), (C<sub>6</sub>H<sub>5</sub>CO<sub>2</sub>)(NMe<sub>4</sub>) (2.5 equiv), and (NMe<sub>4</sub>)OC(CF<sub>3</sub>)<sub>3</sub> (3.0 equiv) in *t*-BuCN (0.1 M) at 90 °C for 20 min. After this time, 5-bromo-*m*-xylene (2 equiv) was added, and then the reaction was stopped after 18 min, which correspond to the last kinetic data point taken into consideration for calculating the KIE (3cb<sub>(18min)</sub> = 11.65%). The reaction was analyzed by calibrated GC-FID revealing only traces of biaryl product (3cb<sub>(18min)</sub> = 0.02%). As this experiment was carried out mimicking the extreme case scenario in which the equilibrium I–IV is totally shifted towards I under the reaction conditions used for the determining the KIE, it further validates that the value of 1.36 is exclusively associated with the cyclometalation step of the benzoate (see SI, section 3).

(14) The  $\sigma_m$  and  $\sigma_p$  values were taken from Hansch, C.; Leo, A.; Taft, R. W. *Chem. Rev.* **1991**, *91*, 165–195.

(15) For leading discussions of the correlation of the rate of electrophilic substitution reaction with Hammett equation, see ref 14 and (a) Hammett, L. P. *J. Am. Chem. Soc.* **1937**, *59*, 96–109. (b) Jaffé, H. H. *Chem. Rev.* **1953**, *53*, 191–261. Brown, H. C.; Okamoto, Y. *J. Am. Chem. Soc.* **1957**, *79*, 1913–1917. (d) Brown, H. C.; Okamoto, Y. *J. Am. Chem. Soc.* **1958**, *80*, 4979–4987. (e) Stock, L. M.; Brown, H. C. *Adv. Phys. Org. Chem.* **1963**, *1*, 35–154. (f) Charton, M. J. *Org. Chem.* **1969**, *34*, 278–285. (g) Gawley, R. E. *J. Org. Chem.* **1981**, *46*, 4595–4597. (h) Santiago, C. B.; Milo, A.; Sigman, M. S. *J. Am. Chem. Soc.* **2016**, *138*, 13424–13430.

(16) (a) Swansburg, S.; Buncel, E.; Lemieux, R. P. *J. Am. Chem. Soc.* **2000**, *122*, 6594–6600. (b) Zdilla, M. J.; Dexheimer, J. L.; Abu-Omar, M. M. *J. Am. Chem. Soc.* **2007**, *129*, 11505–11511. (c) Edwards, D.

R.; Hleba, Y. B.; Lata, C. J.; Calhoun, L. A.; Crudden, C. M. *Angew. Chem., Int. Ed.* **2007**, *46*, 7799–7802. (d) Stokes, B. J.; Richert, K. J.; Driver, T. G. *J. Org. Chem.* **2009**, *74*, 6442–6451. (e) Konnick, M. M.; Decharin, N.; Popp, B. V.; Stahl, S. S. *Chem. Sci.* **2011**, *2*, 326–330. (f) Aihara, Y.; Chatani, N. *Chem. Sci.* **2013**, *4*, 664–670. (g) Neu, H. M.; Yang, T.; Baglia, R. A.; Yosca, T. H.; Green, M. T.; Quesne, M. G.; de Visser, S. P.; Goldberg, D. P. *J. Am. Chem. Soc.* **2014**, *136*, 13845–13852. (h) Kalutharage, N.; Yi, C. S. *J. Am. Chem. Soc.* **2015**, *137*, 11105–11114.

(17) (a) Jaffé, H. H. *J. Am. Chem. Soc.* **1954**, *76*, 4261–4264. (b) Bromilow, R. H.; Kirby, A. J. *J. Chem. Soc., Perkin Trans. 2* **1972**, *2*, 149–155. (c) Hopkins, A. R.; Green, A. L.; Williams, A. J. *Chem. Soc., Perkin Trans. 2* **1983**, *2*, 1279–1283. (d) Craze, G.-A.; Kirby, A. J. *J. Chem. Soc., Perkin Trans. 2* **1974**, *2*, 61–66. (e) Barber, S. E.; Dean, K. E. S.; Kirby, A. J. *Can. J. Chem.* **1999**, *77*, 792–801. (f) Greig, I. R.; Kirby, A. J. *J. Phys. Org. Chem.* **2004**, *17*, 498–506. (g) Edwards, D. R.; Neverov, A. A.; Brown, R. S. *J. Am. Chem. Soc.* **2009**, *131*, 368–377. (h) Jensen, K. H.; Webb, J. D.; Sigman, M. S. *J. Am. Chem. Soc.* **2010**, *132*, 17471–17482.

(18) Davies, D. L.; Macgregor, S. A.; McMullin, C. L. *Chem. Rev.* **2017**, *117*, 8649–8709.

(19) A more stable *mer*-isomer is computed at +7.29 kcal/mol, but the isomerization pathway to form this species involves a transition state at +24.05 kcal/mol, and as such, it is less accessible than the onward PhBr activation via TS(IV'–V'). See Figure S14

(20) A triplet transition state for PhBr activation was located at +61.41 kcal/mol, and the triplet state was also assessed for all isomers of the Ru(II) precursor Int(IV'–V') and found to be very high in energy. Reaction via a triplet spin state can therefore be ruled out (see Figures S5 and S7).

(21) TS<sub>K–L</sub> is in fact slightly higher than the C–Br activation transition state TS<sub>L–M</sub> for all three benzoates. Based on this,  $\Delta G_{\text{span}}$  is 25.57 kcal/mol, 21.84 kcal/mol, and 24.02 kcal/mol for R = H, NMe<sub>2</sub>, and CF<sub>3</sub>, respectively, and thus follows the same trend as the data in the table.

(22) (a) Gorelsky, S. I.; Lapointe, D.; Fagnou, K. *J. Am. Chem. Soc.* **2008**, *130*, 10848–10849. (b) Gorelsky, S. I.; Lapointe, D.; Fagnou, K. *J. Org. Chem.* **2012**, *77*, 658–668.

(23) For a recent example where the net effect of arene *para* substituents is the result of two counter-balancing effects, see: Frasco, D. A.; Mukherjee, S.; Sommer, R. G.; Perry, C. M.; Lambic, N. K.; Abboud, K. A.; Jakubikova, E.; Ison, E. A. *Organometallics* **2016**, *35*, 2435–2445.

(24) (a) Eisenstein, O.; Milani, J.; Perutz, R. N. *Chem. Rev.* **2017**, *117*, 8710–8753. (b) Clot, E.; Eisenstein, O.; Jasim, N.; Macgregor, S. A.; McGrady, J. E.; Perutz, R. N. *Acc. Chem. Res.* **2011**, *44*, 333–348.

(25) (a) Evans, M. E.; Li, T.; Vetter, A. J.; Rieth, R. D.; Jones, W. D. *J. Org. Chem.* **2009**, *74*, 6907–6914. (b) Jones, W. D. *Inorg. Chem.* **2005**, *44*, 4475–4484.

(26) (a) The higher energy of the Ph–Br activation transition state at [Ru(C<sub>6</sub>F<sub>5</sub>)(MeCN)( $\kappa^1$ -PhCO<sub>2</sub>)<sub>2</sub>(PhBr)]<sup>–</sup> compared to [Ru(C<sub>6</sub>F<sub>5</sub>)( $\kappa^2$ -PhCO<sub>2</sub>)( $\kappa^1$ -PhCO<sub>2</sub>)(PhBr)]<sup>–</sup> and [Ru(C<sub>6</sub>F<sub>5</sub>)(MeCN)<sub>2</sub>( $\kappa$ -C,*O*-C<sub>6</sub>H<sub>4</sub>CO<sub>2</sub>)(PhBr)]<sup>–</sup> may reflect the geometry imposed on the metal center by the  $\kappa^2$ -PhCO<sub>2</sub><sup>–</sup> (O–Ru–O = 62°) and cyclometalated (C–Ru–O = 82°) ligands; in comparison the O–Ru–O angle in [Ru(C<sub>6</sub>F<sub>5</sub>)(MeCN)( $\kappa^1$ -PhCO<sub>2</sub>)<sub>2</sub>(PhBr)]<sup>–</sup> is 90°. A similar bite angle effect is known to promote oxidative addition in d<sup>10</sup> ML<sub>2</sub> species by destabilizing an occupied metal-based d $\pi$  orbital.<sup>26b,c</sup> The low symmetry of the current systems causes significant orbital mixing and thus complicates a detailed analysis; however, the average energies of the three occupied d $\pi$  orbitals in [Ru(C<sub>6</sub>F<sub>5</sub>)( $\kappa^2$ -PhCO<sub>2</sub>)( $\kappa^1$ -PhCO<sub>2</sub>)(PhBr)]<sup>–</sup> and [Ru(C<sub>6</sub>F<sub>5</sub>)(MeCN)<sub>2</sub>( $\kappa$ -C,*O*-C<sub>6</sub>H<sub>4</sub>CO<sub>2</sub>)(PhBr)]<sup>–</sup> are 6–7 kcal/mol above those for [Ru(C<sub>6</sub>F<sub>5</sub>)(MeCN)( $\kappa^1$ -PhCO<sub>2</sub>)<sub>2</sub>(PhBr)]<sup>–</sup>, suggesting that a bite angle effect could also contribute to reducing the barrier to Ph–Br activation here. (b) Albright, T. A.; Burdett, J. K.; Whangbo, M. H. *Orbital Interactions in Chemistry*, 2nd ed.; Wiley, New York, 2013. (c) Wolters, L. P.; Bickelhaupt, F. M. In *Computational Studies in Organometallic*



*Chemistry*; Macgregor, S. A., Eisenstein, O., Eds.; Springer International Publishing, 2016; Vol. 167, pp 139–161.

(27) Hoffmann, R.; Howell, J. M.; Rossi, A. R. *J. Am. Chem. Soc.* **1976**, *98*, 2484–2492.

(28) The triplet state of the Ru(II) precursors is always strongly disfavored, so C–Br activation pathways computed on the triplet surface were found to be prohibitively high in energy.

(29) (a) Rousseaux, S.; Gorelsky, S. I.; Chung, B. K. W.; Fagnou, K. *J. Am. Chem. Soc.* **2010**, *132*, 10692–10705. (b) Sun, H.-Y.; Gorelsky, S. I.; Stuart, D. R.; Campeau, L.-C.; Fagnou, K. *J. Org. Chem.* **2010**, *75*, 8180–8189. (c) Zhang, M.; Huang, G. *Chem. - Eur. J.* **2016**, *22*, 9356–9365. (d) Sanhueza, I. A.; Wagner, A. M.; Sanford, M. S.; Schoenebeck, F. *Chem. Sci.* **2013**, *4*, 2767–2775.